Preparation of Dimethyl and Chloro/Methyl Complexes of Platinum(II) Supported by α-Diimine Ligands: Trends in the Ease of Oxidation to Platinum(IV)

by **John D. Scollard**, **Mike Day**, **Jay A. Labinger***, and **John E. Bercaw***

Arnold and Mabel Beckman Laboratories of Chemical Synthesis, California Institute of Technology, Pasadena, CA 91125, USA

Dedicated to the memory of Professor *Luigi M. Venanzi*

α-Diimine ligands react with the platinum(II) alkyl complexes $[(Me_2S)PtMe_2]_2$ and $(Me_2S)_2PtClMe$ to form $(RDAB^{R'})PtMe_2$ and $(RDAB^{R'})PtClMe$ ($RDAB^{R'}$ = RN=CR′–CR′=NR; R = 2,6-Me_2Ph, 2,6-$(CHMe_2)_2$Ph, 3,5-Me_2Ph, 3,5-$(CF_3)_2$Ph, C_6H_{11}; R′ = Me, H). The oxidation of these complexes with Cl_2, I_2, *N*-chlorosuccinimide, $[PtCl_6]^{2-}$ and $(TMEDA)PtMe_2I_2$ has been investigated. Attempts to determine the oxidation potentials of the Pt^{II} complexes electrochemically yielded only irreversible one-electron oxidations. However, a qualitative ordering of increasing difficulty of oxidation has been determined for the series $(RDAB^{R'})PtMe_2 < (RDAB^{R'})PtClMe < (RDAB^{R'})PtCl_2 \ll (RDAB^{R'})PtMe(solvent)]^+$. The oxidation proceeds *via* a two-electron inner-sphere electron transfer from a bridged binuclear intermediate. The oxidation of $(RDAB^{R'})PtMe_2$ by $(TMEDA)PtMe_2I_2$ exhibits characteristic third-order kinetics, first-order each in $[Pt^{II}]$, $[Pt^{IV}]$ and $[I^-]$. Oxidation by a one-electron process in MeCN solution results in a rapid subsequent disproportionation to $Pt^{II}Me$ and $Pt^{IV}Me_3$ cations with MeCN occupying the fourth or sixth coordination sites. Single-crystal X-ray structure determinations for $[(2,6\text{-}Me_2PhDAB^{Me})PtMe_3(MeCN)]^+[PtCl_6]_{0.5}(MeCN)$ and $[(CyDAB^{H})PtMe_3(MeCN)]^+[PtCl_6]_{0.5}(MeCN)$ are reported.

Introduction. – Almost 30 years have passed since *Shilov* and co-workers first reported the oxidation of CH_4 by mixtures of Pt^{II} and Pt^{IV} salts in aqueous solution (*Eqn. 1*) [1]. Since then, the selective catalytic activation and functionalization of alkane C–H bonds have been the focus of substantial efforts [2–4]. Recently, several systems have been developed based on late-transition metals (*e.g.*, Pt, Pd, and Hg) [5–9]. These systems promote electrophilic activation and subsequent oxidation of alkanes. We are currently pursuing new ligand environments for the metal-catalyzed oxidation of alkanes

$$R{-}H + [PtCl_6]^{2-} + H_2O \xrightarrow[120^\circ]{[PtCl_4]^{2-}} R{-}OH + [PtCl_4]^{2-} + 2\ HCl \qquad (1)$$

Late transition metal complexes supported with α-diimine or diamine ligands exhibit behavior relevant to catalytic capabilities. For example, Ni and Pd methyl cations having diimine ancillary ligands have been shown to be highly active catalysts for the polymerization of ethylene and α-olefins [10–18]. Recently, electrophilic Pt cations of the type $[(N{-}N)PtMe(solvent)]^+$ (N–N = diimine, diamine), have been shown to activate C–H bonds [19–24], the first step in the catalytic cycle proposed by *Shilov* and co-workers for his $Pt^{II–IV}$ system (*Scheme 1*). The next step in the cycle involves the oxidation of the resulting Pt^{II} alkyl complex. Mechanistic details of this step have been studied for the original *Shilov* system having only chloro and aquo

ligands [26–28]. Oxidation of the Pt^{II} alkyl complex must compete with the (rapid) protonolysis that would reverse the first step. Furthermore, oxidation of the Pt^{II} alkyl complex must be much more efficient than its Pt^{II} precursor, otherwise all the Pt^{II} will be oxidized to Pt^{IV}, resulting in termination of the catalytic cycle. (In the original *Shilov* system, oxidation by Pt^{IV} regenerates the Pt^{II} catalyst, and this problem does not arise.) Hence, understanding the oxidation chemistry of Pt^{II} α-diimine complexes is crucial for the design of alkane oxidation catalysts based thereon. In this paper, we report the synthesis of a number of such complexes and the results of studies aimed at determining the trends in oxidizability.

Scheme 1

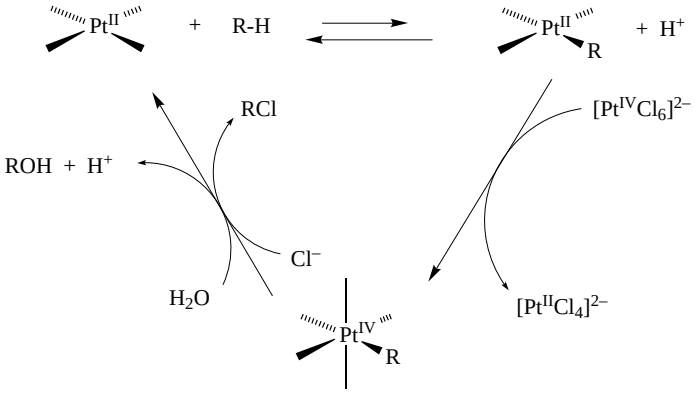

Results and Discussion. – *Synthesis and Characterization of Pt Complexes.* The majority of these Pt complexes are new; therefore, the details of their preparation and characterization will be briefly described. The series of α-diimines, all derivatives of 1,4-diazabutadiene, are generally abbreviated $RDAB^{R'}$, where R is the substitutent on the N-atoms, either a substituted Ph or cyclohexyl, and R′ is the 'backbone' substituent, H or Me. The $Pt^{II}Me_2$ complexes (**1a**–**g**) can be synthesized in 60–95% isolated yield from the α-diimine and $(PtMe_2SMe_2)_2$ (*Scheme 2*). All attempts to prepare complex **1h** resulted in the deposition to metallic Pt. The complexes range in color from forest green to deep purple. The ^{1}H-NMR spectrum of complexes **1a**–**g** indicate C_{2v} symmetry, while the ^{1}H-NMR spectrum of complexes **1c**,**d** also exhibit diastereotopic isopropyl Me resonances, indicating restricted rotation about the N–C_{ipso} bond. The PtMe resonances show ^2J(Pt,H) in the range of 84–87 Hz. In addition, three-bond Pt coupling to the imine backbone protons in the range of 32–34 Hz is observed for complexes **1a**,**1c**, and **1g**.

The platinum methyl chloride complexes **2a**–**h** can be synthesized in 70–95% yield from the corresponding α-diimine and $(Me_2S)_2PtClMe$ in CH_2Cl_2 (*Scheme 3*). This reaction proceeds slowly and requires 4 days in order to achieve high yields. The resulting products are insoluble in aromatic solvents and only partially soluble in CH_2Cl_2. Interestingly, complex **2h** could be synthesized, unlike the dimethyl complex **1h**. The ^{1}H-NMR spectra of complexes **2a**–**h** show C_s symmetry and complexes **2c**,**d**

Scheme 2

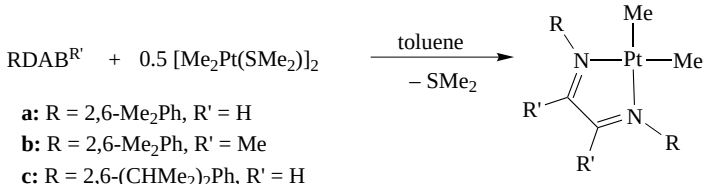

a: R = 2,6-Me_2Ph, R' = H
b: R = 2,6-Me_2Ph, R' = Me
c: R = 2,6-$(CHMe_2)_2$Ph, R' = H
d: R = 2,6-$(CHMe_2)_2$Ph, R' = Me
e: R = 3,5-Me_2Ph, R' = Me
f: R = 3,5-$(CF_3)_2$Ph, R' = Me
g: R = C_6H_{11}, R' = H
h: R = C_6H_{11}, R' = Me

1a–h

also exhibit diastereotopic Me resonances. $^{13}C\{^1H\}$- and $^{195}Pt\{^1H\}$-NMR spectra could not be obtained for complexes **2b**, **2e**, and **2f** due to their insolubility. The $^2J(Pt,H)$ coupling constants of the PtMe groups range from 79–82 Hz, slightly lower than for the corresponding $PtMe_2$ complexes. The $^3J(Pt,H)$ coupling constants for the imine proton *trans* to Me in complexes **2a, 2c**, and **2g** range from 35–38 Hz, while the imine proton *trans* to Cl has $^3J(Pt,H)$ coupling constants in the range of 105–107 Hz. This difference in coupling constants for the imine protons may be attributed to the *trans* influence of the respective ligands. Since Me is a better σ-donor than Cl, it exerts a stronger *trans* influence: the Me group pulls *s* character from the Pt center, resulting in a weakening of the Pt–N bond *trans* to the Me group and a hence-smaller coupling constant.

UV/VIS Spectroscopy. Complexes containing electron-rich metal centers and π-acceptor ligands such as α-diimines often exhibit low-energy solvent-dependent metal-to-ligand charge transfer (MLCT) absorptions. *Fig. 1* illustrates a typical UV/VIS spectrum of a Pt^{II} Me_2 α-diimine and its Pt^{IV} oxidation product. All Pt^{II} spectra exhibit a diimine-centered LL transition, $^1(\pi \rightarrow \pi^*)$ near 370–400 nm. The vibronic structure of this transition is not well-resolved as a result of overlapping charge-transfer transitions. Similar features have been observed in the spectra of $Pt(bpy)Cl_2$ [29] and $Pt(bpy)(pz)_2$ [30]. A second solvent-insensitive band occurs near 215 nm in the spectrum of each complex. This band is assigned to a higher energy spin-allowed LL transition, $^1(\pi \rightarrow \pi_2^*)$, centered on the α-diimine ligand.

At longer wavelengths (500–644 nm), there are two bands that undergo a distinct bathochromic shift with decreasing solvent polarity. In some cases, a shoulder of considerably weaker intensity is observed on the lower-energy band. By analogy to

Scheme 3

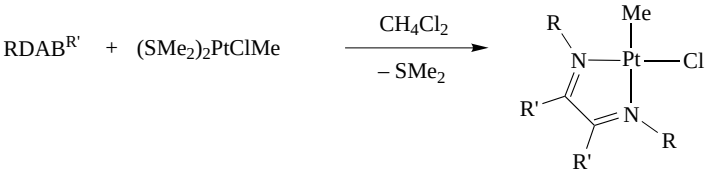

2a–h

Table 1. *NMR Spectroscopic Data for New Complexes*

Complex	^{1}H-NMR[a])		^{13}C-NMR[a])	^{195}Pt-NMR[b])
	PtMe (^2J(Pt,H))	Diimine Me (^3J(Pt,H))	PtMe (^2J(Pt,H))	
1a	1.44 (87)	9.40 (33)	– 13.9 (802)	– 1452
2a	1.20 (81)	8.74 (36), 9.38 (107)	– 11.2 (704)	– 1320
1b	0.79 (87)	1.24	– 14.9 (799)	– 1079
2b	0.72 (79)	1.25,1.66	– [c])	– [c])
1c	1.52 (86)	9.40 (32)	– 13.7 (805)	– 1344
2c	1.30 (84)	8.72 (35), 9.40 (105)	– 10.6 (722)	– 1199
1d	1.80 (86)	50	– 12.5 (811)	– 1309
2d	0.87 (79)	1.29, 1.69	– 11.7 (730)	– 1403
1e	0.90 (87)	1.43	– 13.4[d])	– 1435
2e	0.87 (80)	1.41, 1.83	– [c])	– [c])
1f [23]	1.14 (87)	1.35	– 12.1[d])	– [c])
2f	0.98 (80)	1.33, 1.88	– [c])	– [c])
1g	2.37 (85)	8.17 (34)	– 12.7 (800)	– 1304
2g	1.34 (79)	8.45 (38), 8.89 (107)	– 13.4[d])	– 1111
2h	1.18 (77)	1.84, 1.96	– 12.4 (717)	– 1225

[a]) Chemical shifts δ in ppm relative to TMS; coupling constants J in Hz. [b]) Chemical shifts δ in ppm relative to K_2PtCl_4. [c]) Complex not sufficiently soluble. [d]) Unresolved.

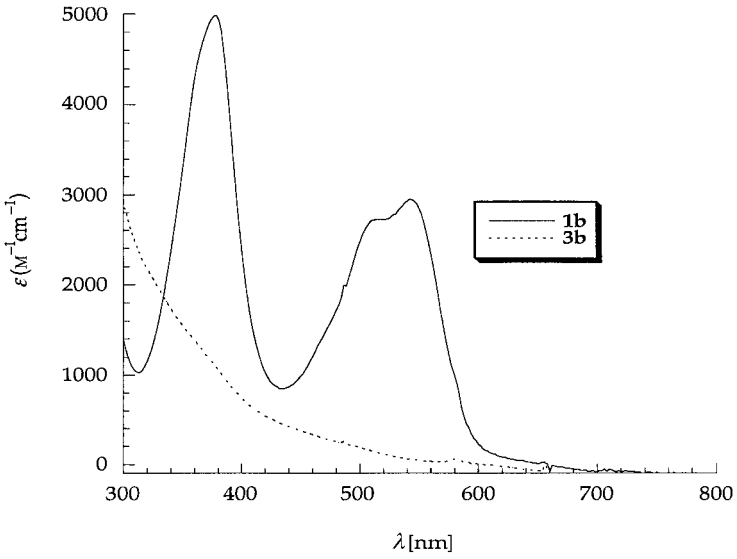

Fig. 1. *UV/VIS Spectra of Complexes* **1a** *and* **3b**

literature assignments for related halo/polypyridine Pt^{II} systems [29][31][32], we attribute the lower-energy band to ^{1}MLCT [d(Pt) $\rightarrow \pi^*$] excitation and the shoulder to the corresponding triplet state. The shift of the lower-energy band ranges from 1190 cm^{-1} to 1580 cm^{-1} when moving from MeCN to toluene for complexes **1a**–**g**. Quantitative analysis of the long-wavelength absorption band was performed for the complex **1b**. Correlation of the energies at the absorption maxima with the empirical

solvent parameter E^*_{MLCT} of *Manuta* and *Lees* [33] led to the graph shown in *Fig. 2*. The solvatochromism of the α-diimine complexes is comparatively strong and quite obvious from color changes between blue and purple, depending on the solvent. The band shifts dramatically to lower energy in less-polar solvents, suggesting considerable charge-transfer character. The negative solvatochromism indicates a polar ground state and a less-polar excited state. Methyl substituents on the α-diimine also result in a small blue shift for these two bands (see *Table 2*). This feature is also consistent with a MLCT transition and has previously been observed in related complexes [30].

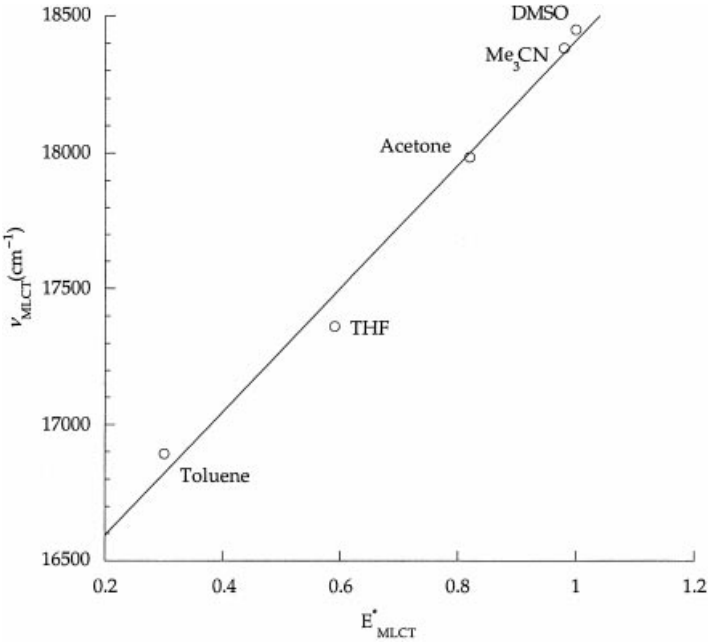

Fig. 2. *Correlation between long-wavelength absorption maxima of complex* **1b** *in different solvents and the solvent parameter* E^*_{MLCT}

Table 2. *UV/VIS Data for Complexes* **1a**–**g**[a])

	MeCN			Toluene	
Complex	$^1(\pi \rightarrow \pi_2^*)$	$^1(\pi \rightarrow \pi^*)$	^{1}MLCT	$^1(\pi \rightarrow \pi^*)$	^{1}MLCT
1a	210 (31.5)	390 (4.4)	584 (2.2)	404 (3.1)	584 (1.9), 632 (2.8)
1b	234 (12.7)	376 (4.8)	514 (2.7), 544 (2.9)	396 (5.2)	546 (2.5), 592 (3.3)
1c	216 (22.6)	392 (4.2)	598 (2.1)	410 (4.9)	592 (1.8), 644 (2.5)
1d	202 (79.8)	382 (3.2)	522 (1.7), 558 (1.9)	398 (5.0)	552 (2.4), 598 (3.2)
1e	– [b])			– [b])	
1f [23]	200 (52.7)	386 (4.1)	560 (2.6)	– [b])	
1g	228 (9.6)	374 (3.2)	528 (2.2)	400 (4.1)	540 (2.1), 576 (2.8)

[a]) λ_{max}, nm (10^3 ε, M^{-1} cm^{-1}). [b]) Insufficiently soluble.

The bleaching of the UV/VIS spectrum upon oxidation from Pt^{II} to Pt^{IV} is also consistent with these assignments. The much higher oxidation potential for Pt^{IV} *vis-a-vis* Pt^{II} blue-shifts the MLCT bands into the UV for the Pt^{IV} complexes.

Oxidation by Halogens. Complexes **1a**–**h** are oxidized by Cl_2 or I_2 to the dihalodimethylplatinum(IV) complexes **3** and **4** (*Scheme 4*). Care must be taken to thoroughly dry the Cl_2 gas, as any moisture present creates HCl, which can protonate the Me groups on platinum to give the $Pt^{IV}Cl_4$ concomitant with the release of CH_4. The addition of halogens always occurs in a *trans* fashion, indicating a stepwise process. Likewise, the chloro(methyl)complexes **2** undergo facile oxidation by Cl_2 or I_2 to form the Pt^{IV} complexes **5** and **6** (*Scheme 5*). Complexes **3** and **5** are microcrystalline yellow solids while the diiodo complexes **4** and **6** are orange solids.

Scheme 4

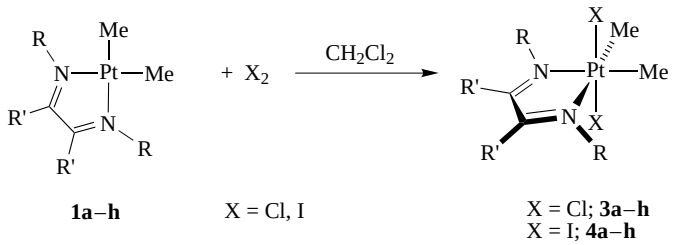

1a–**h** X = Cl, I X = Cl; **3a**–**h**
X = I; **4a**–**h**

Scheme 5

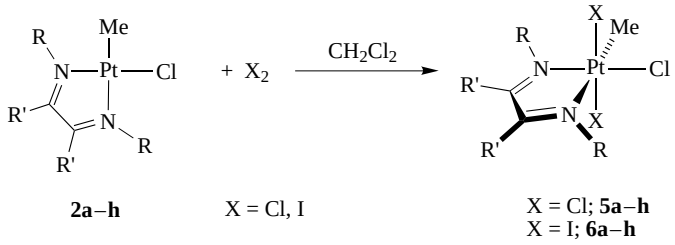

2a–**h** X = Cl, I X = Cl; **5a**–**h**
X = I; **6a**–**h**

Oxidation by N-*Chlorosuccinimide.* Addition of excess *N*-chlorosuccinimide to MeOH solutions of complexes **1** and **2** results in oxidation to the octahedral Pt^{IV} chloro(methoxy)(methyl)complexes **7** and **8**, as evidenced by the rapid bleaching of deeply colored solutions (*Scheme 6*).

In MeCN, cationic $Pt^{IV}Cl(MeCN)$ complexes are formed. Complexes **7** and **8** are yellow powders, and, while attempts to grow single crystals for X-ray-analysis proved impossible, single crystals of **9b** and **9g** were obtained as the $[PtCl_6]^{2-}$ salts (*vide infra*).

Oxidation by Pt^{IV}. The oxidation of complexes **1e**–**h** and **2e**–**h** in MeOH by excess hexachloroplatinate, comparable to the oxidation step in the *Shilov* cycle, results in the formation of complexes **7e**–**h** and **8e**–**h** (*Scheme 7*).

Interestingly, $[PtCl_6]^{2-}$ is unable to oxidize the Pt^{II} complexes supported by α-diimine ligands with 2,6-dimethylphenyl or 2,6-diisopropylphenyl substituents. We believe that the inability of the 2,6-disubstituted aryl group to rotate into the Pt square plane is responsible for the lack of oxidation of complexes **1a**–**d** and **2a**–**d**. Indeed, the

Scheme 6

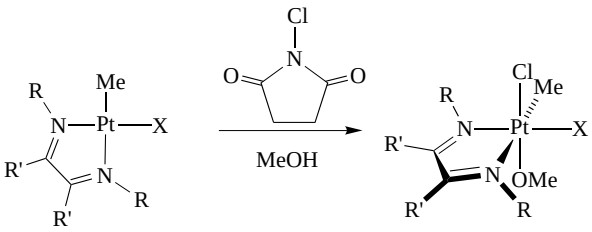

1a–h
2a–h

X = Me; **7a–h**
X = Cl; **8a–h**

Scheme 7

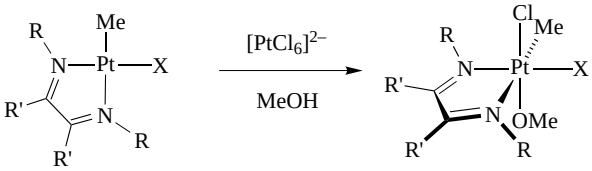

1e–h
2e–h

X = Me; **7e–h**
X = Cl; **8e–h**

3,5-dimethylphenyl-substituted α-diimine complex **1e** is oxidized cleanly while complex **1a** is not. The cyclohexyl-substituted α-diimine complexes **1g**, **2g**, **2h** are also cleanly oxidized. The oxidation by $[PtCl_6]^{2-}$ can also be carried out in MeCN and results in the formation of the cationic Pt^{IV} complexes **9e–h** and **10e–h** (*Scheme 8*). The counter ion in these complexes is 0.5 equivalents of $PtCl_6^{2-}$.

Scheme 8

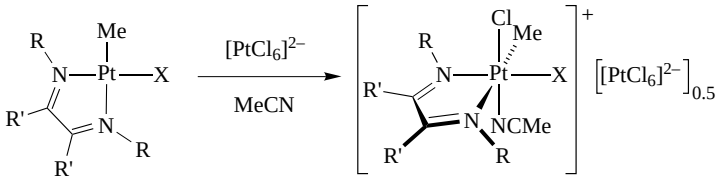

1e–h
2e–h

X = Me; **9e–h**
X = Cl; **10e–h**

Oxidation by (TMEDA)PtI_2Me_2. α-Diimines are modest π-acceptor ligands and are expected to be excellent at stabilizing Pt^{II} complexes. Tetramethylethylenediamine, on the other hand, is a good σ-donor and not a π-acceptor; therefore, tetramethylethylenediamine should be better at stabilizing Pt^{IV} than α-diimines. Nevertheless, compelxes **1e–h** are oxidized cleanly by (TMEDA)PtI_2Me_2 to form the complexes **4e–h** (*Scheme 9*).

Scheme 9

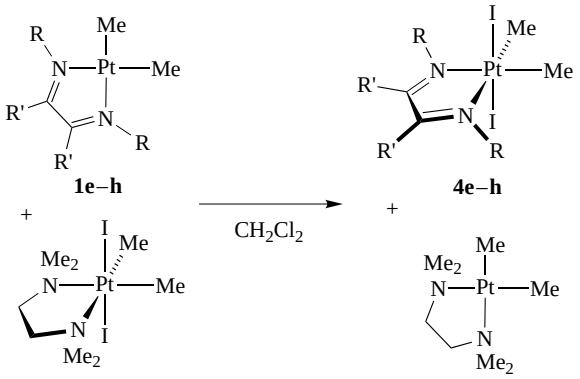

It has been suggested that the Me groups of TMEDA have a significant steric effect on the stability of Pd^{IV} compounds, as they appear to promote the dissociation of I^- from (TMEDA)$PdIMe_3$ [34]. In an attempt to probe the steric effects of the $[NR_2]$ groups, (TMEDA)$PtMe_2$ was treated with (TEEDA)PtI_2Me_2 (TEEDA = tetraethylethylenediamine). Unfortunately, there is no reaction, likely a consequence of excessive steric bulk that blocks approach of the two complexes. Attempts to prepare $[NH_2CH_2CH_2NH_2]PtMe_2$ and $[NH_2CH_2CH_2NH_2]PtI_2Me_2$ to further investigate the importance of steric repulsion between the N-substituents and I^- ligands were unsuccessful.

In contrast, (TMEDA)PtI_2Me_2 is incapable of oxidizing the chloro(methyl) complexes **2a**–**h** (*Scheme 10*). The replacement of a Me by a Cl^- has resulted in a complex that is more difficult to oxidize than the dimethyl complexes. Since a Cl^- group is about the same size as a Me group, this is probably *not* a steric effect; rather, the reduction potentials of complexes **2e**–**h** are likely greater than the reduction potentials of the dimethyl complexes **1e**–**h**.

Scheme 10

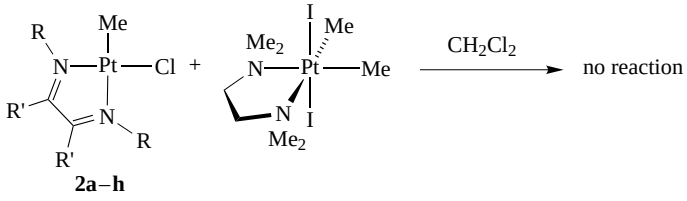

Oxidation Kinetics of Complex **1g**. The rate of the oxidation of complex **1g** by (TMEDA)PtI_2Me_2 was determined (*Scheme 11*). With a large excess of Pt^{IV}, pseudo-first-order rate constants (k_{obs}) were obtained by fitting to a nonlinear least-squares equation 40–60 data points collected over 4–6 half-lives. A typical graph of absorbance *vs.* time for the reaction is shown in *Fig. 3*. The rates are slow (hours) for the reaction at room temperature with no added halide. A summary of the kinetics data appears in *Table 3*.

Scheme 11

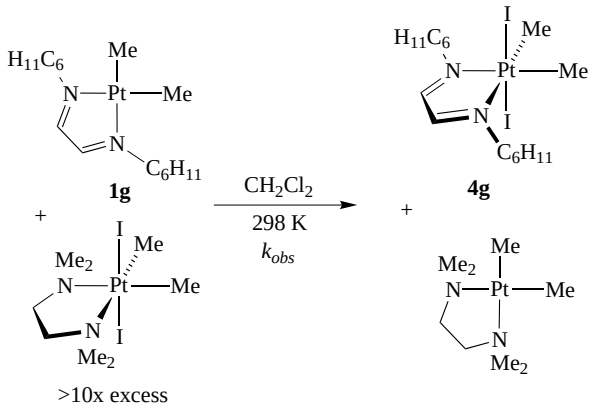

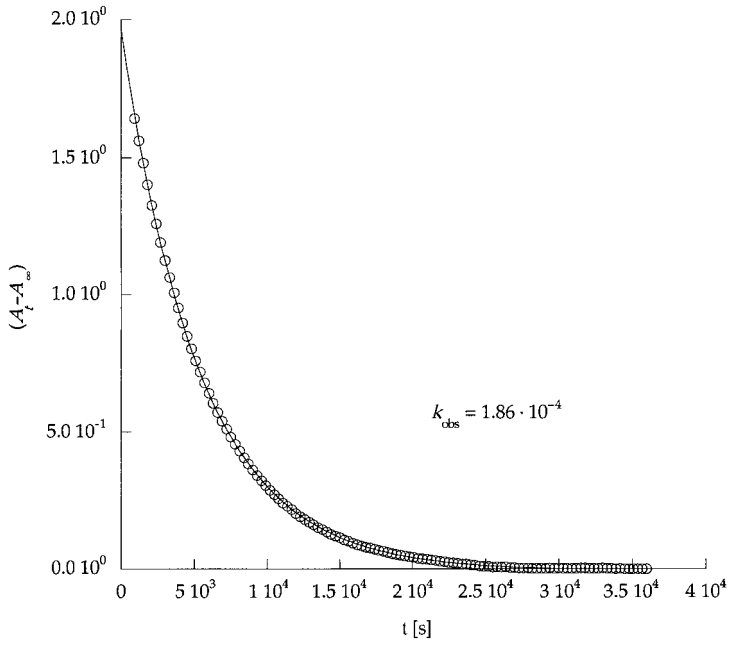

Fig. 3. *Decay of the MLCT band in (CyDAB^H)PtMe$_2$* (**1g**) *during reaction with (TMEDA)PtI$_2$Me$_2$*

The dependence on [Pt^{IV}] for the reaction was determined by varying the concentration of (TMEDA)PtI$_2$Me$_2$. The plot of k_{obs} *vs.* [Pt^{IV}] is shown in *Fig. 4*. The reaction was carried out at constant ionic strength by the addition of 50 equivalents of tetrabutylammonium tetrafluoroborate ((TBA)BF$_4$). A first-order dependence in [Pt^{IV}] is observed for the reaction.

Addition of I$^-$ is found to accelerate the oxidation of complex **1g**. The dependence on I$^-$ was determined by varying [I$^-$] while keeping the ionic strength of the solution

Table 3. *Kinetic Data for the Oxidation of Complex* **1g**

[**1g**]/mM[a])	[(TMEDA)PtI_2Me_2]/mM[a])	[I^-]/mM[a])	*T*/K	k_{obs}/s^{-1}[b])
0.898	8.98	44.9	296.15	0.00366
	18.0			0.00782
	26.9			0.0126
	35.9			0.0166
	44.9			0.0231
0.898	8.98	44.9	296.15	0.00366
		35.9		0.00309
		26.9		0.00230
		18.0		0.00170
		0		0.000186
0.898[c])	8.98[c])	44.9[c])	288.15	0.00537
			298.15	0.00772
			308.15	0.0127
			318.15	0.0180

[a]) In CH_2Cl_2. [b]) $A^{542} = m1 + (m1 - m2)\exp(-k_{obs}(t))$. [c]) In CH_2Cl_2/THF 2:3.

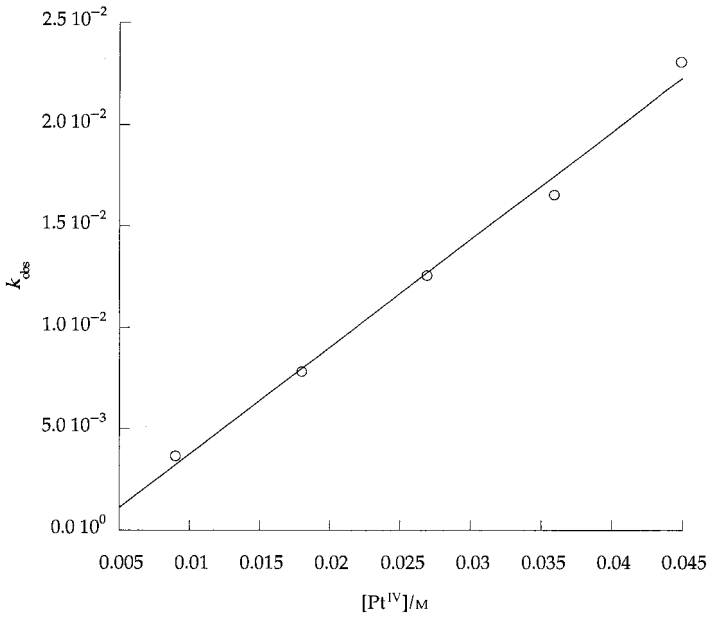

Fig. 4. *Plot of* k_{obs} vs. *[(TMEDA)PtI_2Me_2]*

constant with (TBA)BF_4. A first-order dependence on [I^-] was determined by plotting k_{obs} *vs.* [I^-] (*Fig. 5*).

Thus, the oxidation of ($CyDAB^H$)$PtMe_2$ by (TMEDA)PtI_2Me_2 exhibits characteristic third-order kinetics, first-order each in Pt^{II}, Pt^{IV}, and iodide (*Eqn. 2*):

$$-\frac{d[(CyDAB^H)PtMe_2]}{dt} = k[(CyDAB^H)PtMe_2][(TMEDA)PtI_2Me_2][I^-] \qquad (2)$$

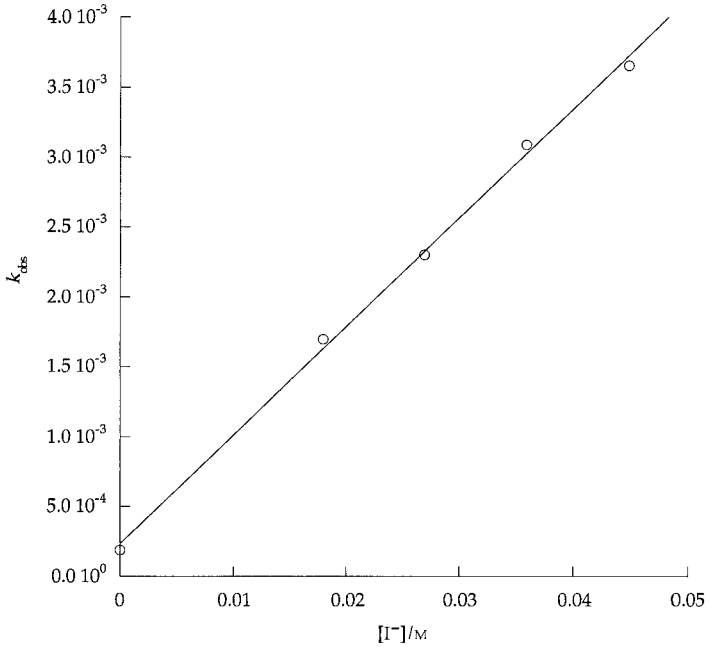

Fig. 5. *Plot of* k_{obs} vs. *[I⁻]*

The mechanism for the oxidation of complex **1g** by (TMEDA)PtI_2Me_2 is shown in *Scheme 12*. The initial step involves a rapidly established equilibrium (K) with I^-, which lies far to the left, to form a five-coordinate Pt^{II} complex. The bimolecular second step (k_1) is assumed to be rate-determining and results in the formation of an iodide-bridged intermediate, which then undergoes a rapid inner-sphere electron transfer followed by dissociation to give the products. Both steric and inductive electronic effects are expected to be important. The former is a direct consequence of the geometry of the bridged complex; bulky in-plane ligands are expected to hinder the bridge formation. If the ligands are bulky enough to prevent the formation of this bridge, no oxidation can occur.

The activation parameters were determined by plotting ln (k_{obs}/T) *vs.* $1/T$ for T over a 30° range (*Fig. 6*). The activation parameters ($\Delta H^{\ddagger} = 6.9$ kcal · mol^{-1}, $\Delta S^{\ddagger} = -45$ e.u.) show that the reaction is characterized by negative entropies of activation and relatively small enthalpies of activation. This behavior is characteristic of an inner-sphere process involving a bridged transition state [35], in agreement with the proposed mechanism and within the range of the activation parameters reported for the ligand exchange at Pt^{IV} catalyzed by Pt^{II} [36].

Electrochemistry. Transition-metal complexes containing α-diimine ligands typically undergo ligand-centered reductions to form species that may be formulated as metal complexes of α-diimine anion radicals. Electrochemical studies of the new complexes were carried out in MeCN/0.1M tetrabutylammonium hexafluorophosphate ((TBA)PF_6) in order to minimize interaction of the coordinatively unsaturated species

Scheme 12

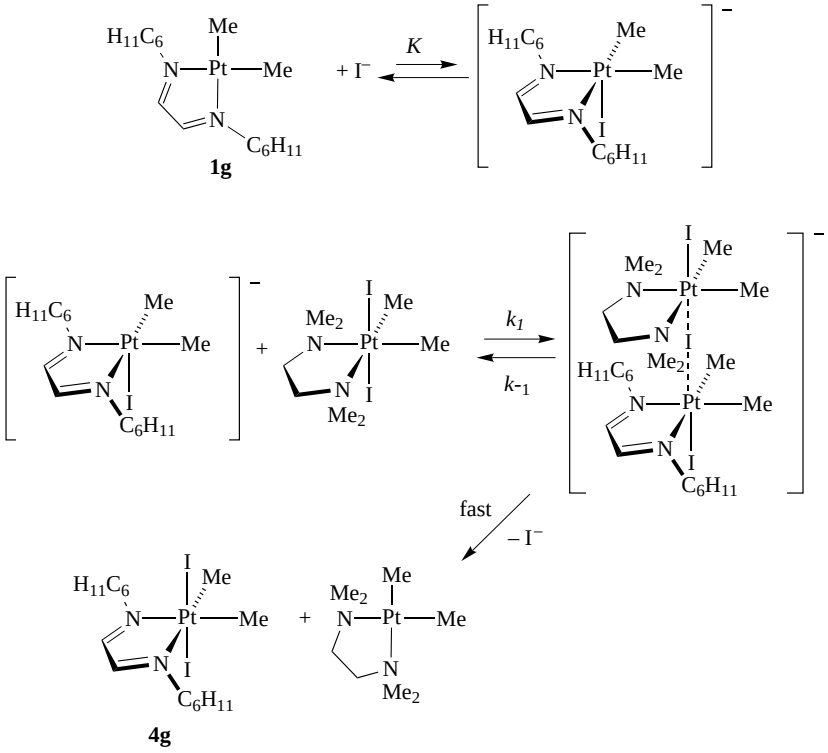

with the electrolyte. *Fig. 7* illustrates a typical cyclic voltammogram, in which there is a reversible one-electron reductive wave, but oxidation gives highly irreversible one-electron waves with strongly solvent-dependent peak potentials, suggesting rapid reaction of the resulting Pt^{III} species. The oxidations remain irreversible even at scan rates as high as 300 V/s. The electrochemical data of complexes supported with α-diimine 2,6-$(CHMe_2)_2$PhDAB^{Me} (**d**) are summarized in *Table 4*.

The single-electron oxidation of Pt^{II} to Pt^{III} was probed chemically. Oxidation of (pen)$PtMe_2$ by ferrocenium hexafluorophosphate results in the formation of a Pt^{III} species followed by rapid disproportionation to cationic Pt^{II} and Pt^{IV} Me species

Table 4. *Comparison of the Irreversible Oxidation Potentials for Pt Complexes Supported with α-Diimine (2,6-$(CHMe_2)_2$PhDAB^{Me})*

Complex	Pt^{II}/Pt^{III} a)b)	1 e^- red a)
(2,6-$(CHMe_2)_2$PhDAB^{Me})$PtMe_2$(**1d**)	611	– 1833
(2,6-$(CHMe_2)_2$PhDAB^{Me})PtClMe (**2d**)	1140	– 1827
(2,6-$(CHMe_2)_2$PhDAB^{Me})$PtCl_2$	1560	– 1821
[(2,6-$(CHMe_2)_2$PhDAB^{Me})PtMe(MeCN)]$^+$	> 2500	– 1825

a) All values in mV and referenced to the Fc/Fc^+ couple. b) Irreversible.

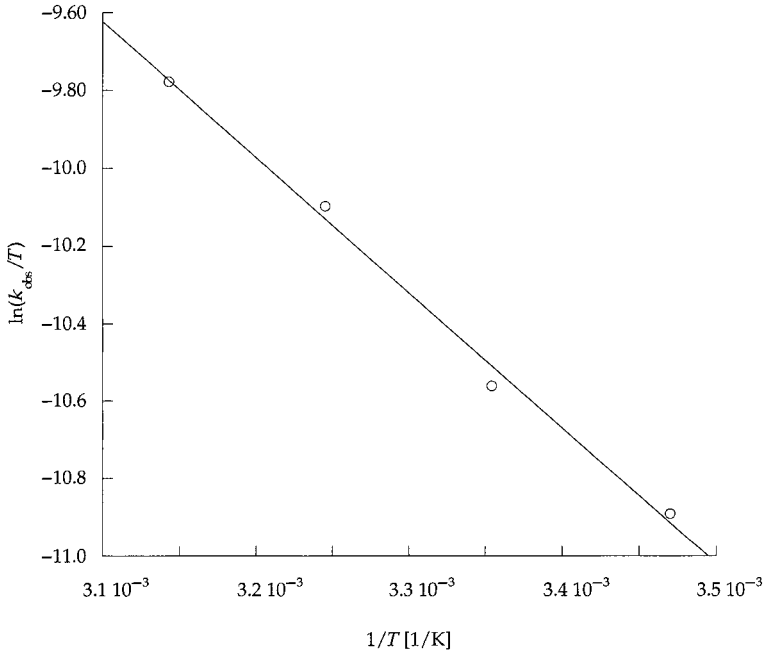

Fig. 6. *Plot of ln* (k_{obs}/T) vs. *1*/T

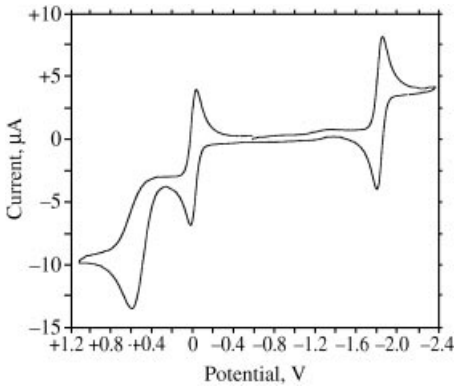

Fig. 7. *Cyclic voltammogram of (2,6-Me_2PhDAB^{Me})PtMe_2* (**1d**; in MeCN/0.1M $Bu_4N^+PF_6^-$ at 10 V/s, internally referenced to Fc/Fc^+ couple)

(*Scheme 13*). Ferrocenium hexafluorophosphate is not a strong enough oxidant to oxidize complexes **1a**–**h**, but bulk electrolysis of MeCN solutions of **1a**–**h** leads to the formation of the cationic Pt^{II} and Pt^{IV} Me complexes (*Scheme 14*). This reactivity pattern was previously established for (RDAB$^{R'}$)$PtMe_2$ by *Tilset* and co-workers [22].

X-Ray Crystallographic Structural Determination of Complexes **9b** *and* **9g**. The molecular structures of complexes **9b** and **9g** were determined crystallographically, and

Scheme 13

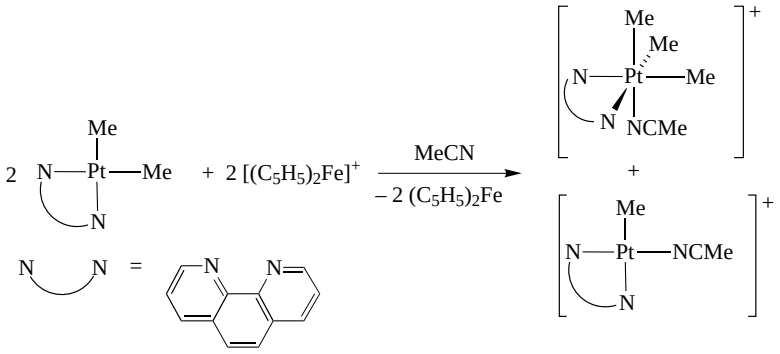

Scheme 14

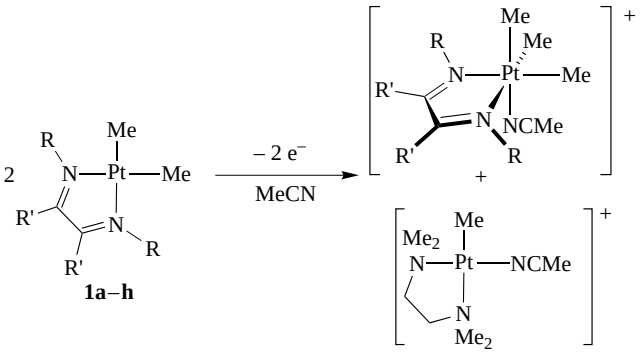

Table 5 contains the experimental and crystallographic data. ORTEP Views of the cations are shown in *Figs. 8* and *9*, and selected bond distances and angles are listed in *Table 6*.

The molecular structure of complex **9b** consists of discrete platinum cationic units of $[C_{24}H_{33}ClN_3Pt]^+$, sitting at a general position, and the counterion, $[PtCl_6]^{2-}$, sitting at a center of symmetry. The Pt-atom of the cation displays predominately octahedral geometry. The N(1)–Pt(1)–N(2) angle is constrained to 75.3° as a consequence of the α-diimine ligand's two-C-atom bridge. The sum of the angles around the Pt-atom in the $[N_2PtC_2]$ plane is 359.9°. The average Pt–C bond length of 2.059 Å and Pt–N bond length of 2.21 Å are comparable to the bond lengths of similar complexes reported by *Tilset* and co-workers [22] and others [37–39]. The Pt–MeCN bond distance is noticeably shorter in complex **9b** due to a smaller *trans*-influence exerted from the Cl^- ligand relative to Me. The planes of the arene rings are rotated relative to the $[N_2PtC_2]$ plane by an average of 98° and are within 3.2° of being coplanar. This feature is similar to other α-diimine Pt [40][41] and Pd [42][43] complexes, but is unlike the complex of *Tilset* and co-workers, where the arene rings are oriented 81.8° from each other. The hexachloroplatinate anion is unexceptional, and the structure exhibits no unusual intermolecular contacts.

Table 5. *Crystal Data and Structure Refinement for Complexes* **9b** *and* **9g**

	9b	**9g**
Empirical formula	$[C_{24}H_{33}ClN_3Pt]_2]PtCl_6] \cdot 2$ MeCN	$[C_{18}H_{33}ClN_3Pt]_2[PtCl_6] \cdot 2$ MeCN)
T [K]	85	85
Formula weight [g mol^{-1}]	1678.06	1533.92
Unit-cell dimensions		
a [Å]	33.152(26)	9.609(4)
b [Å]	9.561(4)	10.918(5)
c [Å]	20.226(17)	13.468(5)
α [°]		94.04(3)
β [°]	113.54(6)	105.34(3)
γ [°]		101.43(4)
V [Å^3]	5877(6)	1324.2(10)
Z	8	1
Crystal system	Monoclinic	Triclinic
Space group	$C2/c$	$P\bar{1}$
Data/Restraints/Parameters	5178/0/321	4631/0/268
Goodness-of-fit (obs. data)	2.296	1.357
Final R indices (obs. data)	$R1 = 0.0403$, $wR2 = 0.0791$	$R1 = 0.0272$, $wR2 = 0.0520$
R indices (all data)	$R1 = 0.0365$, $wR2 = 0.0546$	$R1 = 0.0508$, $wR2 = 0.0804$

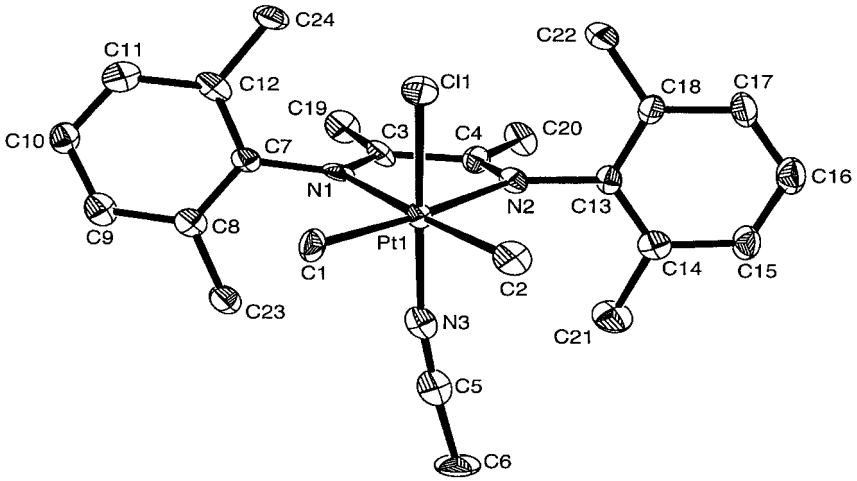

Fig. 8. *Labeled ORTEP-3* [51] *view of the* **9b** *cation*. Thermal ellipsoids drawn at 60% probability; H-atoms omitted for clarity.

The molecular structure of complex **9g** is similar to that of **9b**. The asymmetric unit consists of the discrete Pt cation $[C_{18}H_{33}ClN_3Pt]^+$, sitting at a general position, and a $[PtCl_6]^{2-}$ anion, sitting at a center of symmetry. The geometry of the Pt cation is essentially octahedral with the (N1)–Pt–N(2) angle restricted to 76.1°. The bond distances and angles are very close to those for complex **9b**. The cyclohexyl groups are oriented pseudo orthogonal to each other, similar to the related complex (Cy-DAB^H)PtMe$_4$ [37]. The cyclohexyl groups, being less sterically demanding than the 2,6-

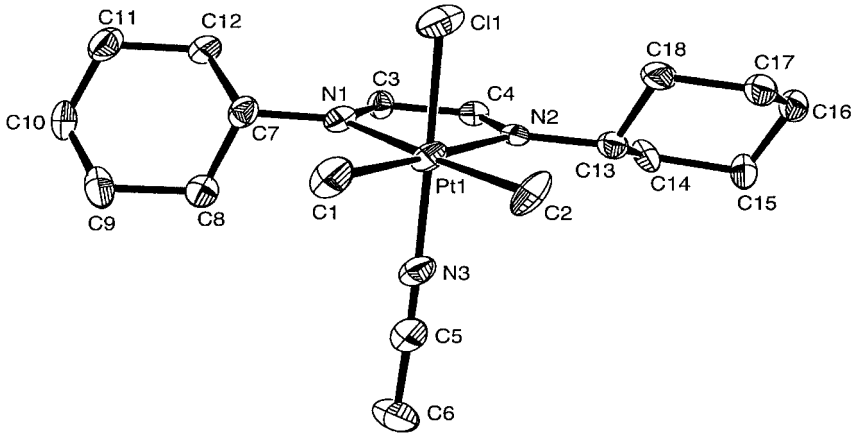

Fig. 9. *Labeled ORTEP-3* [51] *view of the* **9g** *cation*. Thermal ellipsoids drawn at 60% probability; H-atoms omitted for clarity.

Table 6. *Selected Bond Lengths* [Å] *and Angles* [°]

	9b	**9g**
Pt–C(1)	2.061(7)	2.051(6)
Pt–C(2)	2.057(7)	2.057(5)
Pt–N(1)	2.196(6)	2.176(4)
Pt–N(2)	2.221(6)	2.172(4)
Pt–Cl(1)	2.290(2)	2.2854(17)
Pt–N(3)	1.982(7)	1.976(5)
N(1)–C(3)	1.278(9)	1.272(7)
N(2)–C(4)	1.281(9)	1.268(6)
C(3)–C(4)	1.521(10)	1.464(7)
N(1)–C(7)	1.453(9)	1.469(7)
N(2)–C(13)	1.462(9)	1.479(7)
N(1)–Pt–N(2)	75.3(2)	76.14(16)
N(1)–Pt–C(1)	98.4(3)	100.2(2)
C(1)–Pt–C(2)	87.1(3)	85.2(2)
N(2)–Pt–C(2)	99.2(3)	98.5(2)
Cl(1)–Pt–N(3)	173.46(17)	178.28(14)
Pt–N(1)–C(7)	123.6(4)	125.2(3)
Pt–N(2)–C(13)	124.4(3)	126.3(4)
C(1)–Pt–N(2)	176.26(19)	173.7(3)
C(1)–Pt–N(1)	174.6(2)	174.5(3)

dimethylphenyl groups of complex **9b**, can rotate freely into the $[N_2PtC_2]$ plane to reduce steric congestion, while, in complex **9b**, the Ph groups are both locked in positions orthogonal to the $[N_2PtC_2]$ plane. The hexachloroplatinate anion exhibits no unusual intermolecular contacts.

Conclusions. – Platinum(II) alkyl complexes supported by α-diimine ligands, $(RDAB^{R'})PtMe_2$ and $(RDAB^{R'})PtClMe$, have been prepared, and the relative ease of oxidation has been investigated. Oxidation by halogens to the corresponding *trans*-

dihalo Pt^{IV} complexes proceeds rapidly for all complexes examined, whereas, with *N*-chlorosuccinimide, the chloro/solvento Pt^{IV} complexes are generated. With hexachloroplatinate, only the less-crowded members of the series are oxidized. Interestingly, and counter to our expectations based on ligand electronic effects, the less-crowded $(RDAB^{R'})PtMe_2$ complexes react, essentially completely, with $(TMEDA)PtI_2Me_2$ to form $(RDAB^{R'})PtI_2Me_2$ and $(TMEDA)PtMe_2$. Unfavorable steric interactions between the TMEDA Me groups and the iodide ligands for $(TMEDA)PtI_2Me_2$ appear to be responsible, favoring the less-crowded Pt^{II} and Pt^{IV} products. Studies of the mechanism for this reaction with $(CyDAB^{H})PtMe_2$ indicate a two-electron inner-sphere electron transfer with the usual third-order kinetics, consistent with generation of the reactive iodide-bridged $\{(TMEDA)Me_2IPt\cdots I\cdots Pt(CyDAB^{H})Me_2I\}$-activated complex. Attempts to determine the oxidation potentials of the Pt^{II} complexes electrochemically yielded only irreversible one-electron oxidations, so that thermodynamic potentials for the Pt^{II}/Pt^{IV} couples could not be obtained *via* electrochemistry. However, a qualitative ordering of oxidation potentials has been determined for the series $(RDAB^{R'})PtMe_2 < (RDAB^{R'})PtMeCl < (RDAB^{R'})PtCl_2 \ll (RDAB^{R'})PtMe(solv)]^+$. Oxidation by one-electron processes in MeCN solution results in a rapid subsequent disproportionation to Pt^{II} Me and Pt^{IV} Me_3 trimethyl cations with MeCN occupying the fourth or sixth coordination sites. Single-crystal X-ray structure determinations for $[(2,6\text{-}Me_2PhDAB^{Me})PtMe_3(MeCN)]^+[PtCl_6]_{0.5}$(-MeCN) and $[(CyDAB^{H})PtMe_3(MeCN)]^+[PtCl_6]_{0.5}(MeCN)$ have been determined.

Experimental Part

General. All experiments were performed under dry Ar with standard *Schlenk* techniques unless otherwise noted. THF, petroleum ether (p.e.), Et_2O, and benzene were distilled from Na/benzophenone ketyl under N_2. Toluene was distilled from molten Na, MeOH from Mg turnings, MeCN and CH_2Cl_2 from CaH_2 under Ar and stored over activated 4 Å molecular sieves. K_2PtCl_4 and K_2PtCl_6 were obtained from *Pressure Chemical*. All other reagents were obtained from *Aldrich* and used as received except as noted. *N,N,N′,N′*-Tetramethylethylenediamine (TMEDA), 2,6-diisopropylaniline, and 2,6-dimethylaniline were distilled prior to use. α-Diimines [44][45], $Pt(SMe_2)_2MeCl$, and $[Me_2Pt(SMe_2)]_2$ [46] were synthesized according to lit. procedures. ^1H-(500.168 MHz), ^{13}C- (125.781 MHz), and ^{195}Pt- (107.25 MHz) NMR spectra were recorded in CD_2Cl_2, C_6D_6, or (D_6)acetone at approximately 20° on a *Varian Unity-500* spectrometer. The chemical shifts (δ) in ppm were referenced to internal $CDHCl_2$ (5.32), C_6D_5H (7.15) or CD_3COCD_2H (2.04 for ^1H) and to CD_2Cl_2 (54.0), C_6D_6, (128.0) or CD_3COCD_3 (29.9) for ^{13}C; ^{195}Pt signals were referenced externally to K_2PtCl_4 (-1935); coupling constants (J) in Hz. Electrochemical experiments were carried out on a *BAS100* instrument with $(TBA)PF_6$ electrolyte and a Pt electrode. Elemental analyses were performed by Mr. *Fenton Harvey* at the California Institute of Technology or by *Midwest Microlab* (Indianapolis, IN).

Kinetics. Stock solns. of the reactants were prepared by weighing samples and dissolving in CH_2Cl_2 or CH_2Cl_2/THF 2:3 as indicated in *Table 3*. A constant ionic strength of 44.9 mM was maintained by the addition Bu_4NI and/or Bu_4NBF_4. The reactions were started by mixing appropriate volumes of freshly prepared stock solns. of the reactants in a 1 cm quartz cell maintained in the thermostat-controlled cell compartment of a *Hewlett-Packard HP8452A* diode-array spectrophotometer. The progress of the reaction was monitored at appropriate time intervals by recording the absorbance at 542 nm. Under kinetics conditions, the starting $[Pt^{II}]$ was always < 0.9 mM and at least $10\times$ lower than the $[Pt^{IV}]$. It was found that the reactions obey a pseudo-first-order rate law over the entire course of the reaction. Pseudo-first-order rate constants, k_{obs}, were evaluated by fitting a nonlinear least-squares equation to the plots of $(A_t - A_\infty)$ against time, where A_t and A_∞ are the absorbance of the reacting mixture at time t and at the end of the reaction, resp. The activation parameters were calculated from the gradient and intercept of the plot of $\ln(k_{obs}/T)$ *vs.* $1/T$ over a 30° temp. range.

General Procedure for the Synthesis of (RDAB$^{R'}$)PtMe$_2$ (**1a**–**h**). $[Me_2Pt(SMe_2)]_2$ (250 mg, 0.435 mmol) was dissolved in toluene (20 ml). α-Diimine **a**–**h** (0.870 mmol) was added as a solid. The soln. became deep purple

or deep green (depending on the α-diimine) after a few minutes. The mixture was stirred overnight at r.t. The solvent was reduced, and the resulting product was precipitated by the addn. of p.e. Products were collected by filtration in 60% – 95% yields.

General Procedure for the Synthesis of (RDAB$^{R'}$)PtCl (**2a**–**h**). $Pt(SMe_2)_2ClMe$ (250 mg, 0.676 mmol) was dissolved in CH_2Cl_2 (10 ml). α-Diimine **a**–**h** (0.676 mmol) was added as a solid. The soln. turned reddish purple after a few min. The mixture was stirred 4 d at r.t. The solvent was reduced, and p.e. was added to precipitate the product. The product was collected by filtration and washed with cold p.e. Yields ranged from 70 – 95%.

Alternative Procedure for the Synthesis of **2a**–**h**. Complex **1a** (100 mg, 0.204 mmol) was dissolved in toluene, and HCl in Et_2O (0.1M, 2.20 ml, 0.22 mmol) was added *via* syringe. The soln. became cloudy with a yellow precipitate after a few min. The mixture was stirred overnight at r.t., the solvent was reduced, and the resulting product was collected by filtration and washed with cold p.e. Yields ranged from 75 – 90%.

Typical Procedure for [(RDAB$^{R'}$)PtCl$_2$Me$_2$ (**3a**). Complex **1a** (50 mg, 0.102 mmol) was dissolved in CH_2Cl_2 (15 ml). Gaseous Cl_2, filtered through activated basic alumina, was introduced into the reaction. The soln. became light yellow almost immediately. The solvent was reduced and the resulting product was precipitated by the addn. of p.e. Products were collected by filtration in 80% – 95% yields.

Typical Procedure for [(RDAB$^{R'}$)PtI$_2$Me$_2$ (**4g**). Complex **1g** (50 mg, 0.11 mmol) was dissolved in CH_2Cl_2 (10 ml). Excess I_2 was added as a solid. The soln. became light yellow after a few min, then purple as the excess I_2 dissolved. The mixture was stirred 1 h at r.t. The excess I_2 was reduced by addn. of a sat. aq. soln. of $Na_2S_2O_3$ (10 ml). The org. layer was separated and the aq. layer extracted with CH_2Cl_2 (3×10 ml). The solvent was dried over anh. Na_2SO_4, reduced in volume, and the resulting product was precipitated by the addn. of p.e. Products were collected by filtration in 80% – 95% yields.

Typical Procedure for [(RDAB$^{R'}$)PtCl(OMe)Me$_2$ (**7a**). Complex **1a** (50 mg, 0.102 mmol) was dissolved in MeOH (15 ml). *N*-Chlorosuccinimide (15 mg, 0.11 mmol) was added as a solid. The soln. turned pale yellow after a few min. The mixture was stirred 3 h at r.t. The solvent was reduced and the resulting product was precipitated by the addn. of p.e. Products were collected by filtration in 60% – 95% yields.

Typical Procedure for [(RDAB$^{R'}$)PtClMe$_2$(MeCN)]$_2$(PtCl$_6$) (**9g**). Complex **1g** (50 mg, 0.11 mmol) was dissolved in MeCN (15 ml). K_2PtCl_6 (121 mg, 0.25 mmol) was added as a solid. The soln. turned pale yellow and cloudy after *ca.* 1 h. The mixture was stirred overnight at r.t. The solvent was replaced with toluene and filtered through *Celite*. The resulting product was recrystallized from a mixture of toluene and p.e. Products were collected by filtration in 42% – 60% yields.

Data of (2,6-Me$_2$DAB^H)PtMe$_2$ (**1a**). Deep green solid. Yield 362 mg (0.74 mmol, 85%). ^{1}H-NMR (C_6D_6): 9.40 (*s*, 2 H–C=N, ^3J(Pt,H) = 33); 7.20 (*m*, 6 arom. H); 2.24 (*s*, 12 H, Ph*Me*$_2$); 1.4 (*s*, $PtMe_2$, ^2J(Pt,H) = 87). ^{13}C{^{1}H}-NMR (CD_2Cl_2): 163.5; 149.0; 129.7; 127.1; 126.9; 17.7; –13.9 (^1J(Pt,C) = 802). ^{195}Pt{^{1}H}-NMR (CD_2Cl_2): –1452. Anal. calc. for $C_{20}H_{26}N_2Pt$: C 49.07, H 5.35, N 5.72; found: C 49.49, H 5.17, N 5.56.

Data of (2,6-Me$_2$PhDAB^{Me})PtMe$_2$ (**1b**). Deep purple solid. Yield 356 mg (0.69 mmol, 79%). ^{1}H-NMR (CD_2Cl_2): 7.20 (*m*, 4 arom. H); 7.13 (*m*, 2 arom. H); 2.16 (*s*, 12 H, Ph*Me*$_2$); 1.24 (*s*, 2 *Me*–C=N); 0.79 (*s*, $PtMe_2$, ^2J(Pt,H) = 87). ^{13}C{^{1}H}-NMR (CD_2Cl_2): 170.6; 146.2; 129.2; 128.2; 126.3; 20.2; 17.5; –14.9 (^1J(Pt,C) = 799). ^{195}Pt{^{1}H}-NMR (C_6D_6) –1079. Anal. calc. for $C_{22}H_{30}N_2Pt$: C 51.05, H 5.84, N 5.41; found: C 50.88, H 5.55, N 5.38.

Data of (2,6-(CHMe$_2$)$_2$PhDAB^H)PtMe$_2$ (**1c**). Deep green solid. Yield 366 mg (0.61 mmol, 70%). ^{1}H-NMR (CD_2Cl_2): 9.40 (*s*, ^3J(Pt,H) = 32, 2 H–C=N); 7.32 (*m*, 6 arom. H); 3.24 (*septet*, 4 C*H*Me_2); 1.52 (*s*, ^2J(Pt,H) = 86, $PtMe_2$); 1.30 (*d*, 12 H, CH*Me*$_2$); 1.13 (*d*, 12 H, CH*Me*$_2$). ^{13}C{^{1}H}-NMR (CD_2Cl_2): 163.4; 146.5; 140.4; 127.7; 123.4; 28.1; 24.9; 23.1; –13.7 (^1J(Pt,C) = 805). ^{195}Pt{^{1}H}-NMR (CD_2Cl_2): –1344. Anal. calc. for $C_{28}H_{42}N_2Pt$: C 55.89, H 7.04, N 4.66; found: C 55.64, H 6.64, N 4.50.

Data of (2,6-(CHMe$_2$)$_2$PhDAB^{Me})PtMe$_2$ (**1d**). Deep purple solid. Yield 329 mg (0.52 mmol, 0.60%). ^{1}H-NMR (C_6D_6): 7.19 (*m*, 6 arom. H); 3.18 (*septet*, 4 C*H*Me_2); 1.80 (*s*, ^2J(Pt,H) = 86, $PtMe_2$); 1.36 (*d*, 12 H, CH*Me*); 1.01 (*d*, 12 H, CH*Me*); 0.50 (*s*, 2 Me–C=N). ^{13}C{^{1}H}-NMR (C_6D_6): 169.8; 144.3; 139.6; 128.2; 124.0; 28.4; 24.1; 24.0; 21.3; –12.5 (^1J(Pt,C) = 811 Hz). ^{195}Pt{^{1}H}-NMR (C_6D_6): –1309. Anal. calc. for $C_{30}H_{46}N_2Pt$: C 57.21, H 7.36, N 4.45; found: C 56.99, H 6.85, N 4.36.

Data of (3,5-Me$_2$PhDAB^{Me})PtMe$_2$ (**1e**). Purple solid (428 mg, 0.83 mmol, 95%). ^{1}H-NMR (C_6D_6): 6.92 (*s*, 2 arom. H); 6.61 (*s*, 4 arom. H); 2.36 (*s*, 12 H, Ph*Me*$_2$), 1.43 (*s*, 2 Me–C=N); 0.90 (*s*, ^2J(Pt–H) = 87, $PtMe_2$). ^{13}C{^{1}H}-NMR (CD_2Cl_2): 171.0; 148.2; 139.0; 128.0; 119.8; 21.7; 21.2; –13.4 (^1J(Pt,C) unresolved). ^{195}Pt{^{1}H}-NMR (CD_2Cl_2): –1435. Anal. calc. for $C_{22}H_{30}N_2Pt$: C 51.05, H 5.84, N 5.41; found: C 50.88, H 5.87, N 5.25.

Data of (CyDAB^H)PtMe$_2$ (**1g**). Deep purple solid. Yield 322 mg (0.72 mmol, 83%). ^{1}H-NMR (C_6D_6): 8.17 (*s*, ^3J(Pt,H) = 34, 2 CH); 4.24 (*m*, 2 H–C=N); 2.37 (*s*, ^2J(Pt,H) = 85, $PtMe_2$); 2.08 (*m*, 2 CH_2); 1.55 (*m*, 2 CH_2); 1.46 (*m*, CH_2); 1.23 (*m*, 2 CH_2); 1.03 (*m*, 2 CH_2); 0.91 (*m*, CH_2). ^{13}C{^{1}H}-NMR (C_6D_6): 157.6; 65.4; 34.3; 26.4;

26.1; −12.7 (^1J(Pt,C) = 800). ^{195}Pt{^{1}H}-NMR (C_6D_6): −1304. Anal. calc. for $C_{16}H_{30}N_2Pt$: C 43.14, H 6.79, N 6.29; found: C 43.06, H 6.24, N 6.29.

Data of (2,6-Me$_2$PhDAB^H)PtClMe (**2a**): Purple solid. Yield 296 mg (0.58 mmol, 86%). ^{1}H-NMR (C_6D_6): 9.38 (*s*, ^3J(Pt,H) = 107, H−C=N); 8.74 (*s*, ^3J(Pt,H) = 36, H−C=N); 7.24 (*s*, 3 arom. H); 7.19 (*s*, 3 arom. H); 2.30 (*s*, PhMe$_2$); 2.27 (*s*, PhMe$_2$); 1.20 (*s*, ^2J(Pt,H) = 81, PtMe$_2$). ^{13}C{^{1}H}-NMR (CD_2Cl_2): 165.5; 164.5; 148.2; 147.7; 131.0; 129.5; 128.5; 128.4; 128.2; 127.7; 18.3; 17.5; −11.2 (^1J(Pt,C) = 704). ^{195}Pt{^{1}H}-NMR (CD_2Cl_2): −1320. Anal. calc. for $C_{19}H_{25}ClN_2Pt$: C 44.75, H 4.55, N 5.49; found: C 44.21, H 4.20, N 5.22.

Data of (2,6-Me$_2$PhDAB^{Me})PtClMe (**2b**). Purple solid. Yield 345 mg (0.64 mmol, 95%). ^{1}H-NMR (C_6D_6): 7.25–7.14 (*m*, 6 arom. H); 2.22 (*s*, PhMe$_2$); 2.20 (*s*, PhMe$_2$); 1.66 (*s*, Me−C=N); 1.25 (*s*, Me−C=N); 0.72 (*s*, ^2J(Pt,H) = 79, PtMe). Anal. calc. for $C_{19}H_{25}ClN_2Pt$: C 46.88, H 5.06, N 5.21; found: C 46.88, H 4.69, N 5.11.

Data of (2,6-(CHMe$_2$)$_2$PhDAB^H)PtClMe (**2c**). Purple solid. Yield 345 mg (0.55 mmol, 82%). ^{1}H-NMR (CD_2Cl_2): 9.40 (*s*, ^3J(Pt,H) = 105, H−C=N); 8.72 (*s*, ^3J(Pt,H) = 35, H−C=N); 7.35 (*m*, 4 arom. H); 7.28 (*m*, 2 arom. H); 3.22 (*m*, 4 C*H*Me$_2$); 1.35 (*d*, 6 H, CH*Me*); 1.34 (*d*, 6 H, CH*Me*); 1.30 (*s*, ^2J(Pt,H) = 84, PtMe); 1.16 (*d*, 6 H, CH*Me*); 1.16 (*d*, 6 H, CH*Me*). ^{13}C{^{1}H}-NMR (CD_2Cl_2): 165.1; 164.1; 145.7; 144.9; 141.5; 140.1; 129.2; 128.4; 124.0; 123.5; 28.8; 28.2; 24.9; 24.6; 23.4; 23.0; −10.6 (^1J(Pt,C) = 722). ^{195}Pt{^{1}H}-NMR (CD_2Cl_2): −1199. Anal. calc. for $C_{27}H_{39}ClN_2Pt$: C 52.12, H 6.32, N 4.50; found: C 52.19, H 6.19, N 4.26.

Data of (2,6-(CHMe$_2$)$_2$PhDAB^{Me})PtClMe (**2d**). Orange-red solid. Yield 308 mg (0.47 mmol, 70%). ^{1}H-NMR (C_6D_6): 7.34 (*m*, 3 arom. H); 7.29 (*m*, 3 arom. H); 3.03 (*septet*, 2 C*H*Me$_2$); 3.02 (*septet*, 2 C*H*Me$_2$); 1.69 (*s*, Me−C=N); 1.35 (*d*, 6 H, CH*Me*); 1.33 (*d*, 6 H, CH*Me*); 1.29 (*s*, Me−C=N); 1.16 (*d*, 6 H, CH*Me*); 1.15 (*d*, 6 H, CH*Me*); 0.87 (*s*, ^2J(Pt,H) = 79, PtMe). ^{13}C{^{1}H}-NMR (C_6D_6): 174.4; 172.5; 142.6; 140.5; 139.6; 128.7; 127.8; 124.4; 123.7; 28.9; 28.3; 24.1; 24.0; 23.9; 23.6; 22.3; 20.5; −11.7 (^1J(Pt,C) = 730). ^{195}Pt{^{1}H}-NMR (C_6D_6): −1403. Anal. calc. for $C_{29}H_{45}ClN_2Pt$: C 53.57, H 6.67, N 4.31; found: C 53.19, H 6.53, N 4.15.

Data of (3,5-Me$_2$PhDAB^{Me})PtClMe (**2e**). Purple solid. Yield 335 mg (0.62 mmol, 92%). ^{1}H-NMR (C_6D_6): 6.98 (*s*, 1 arom. H); 6.97 (*s*, 1 arom. H); 6.70 (*s*, 2 arom. H); 6.64 (*s*, 2 arom. H); 2.38 (*s*, PhMe$_2$); 2.38 (*s*, PhMe$_2$); 1.83 (*s*, Me−C=N); 1.41 (*s*, Me−C=N); 0.87 (*s*, ^2J(Pt,H) = 80, PtMe). Anal. calc. for $C_{21}H_{27}ClN_2Pt$: C 46.88, H 5.06, N 5.21; found: C 46.82, H 4.67, N 4.92.

Data of 3,5-(CF$_3$)$_2$ PhDAB^{Me})PtClMe (**2f**). Purple solid. Yield 377 mg (0.50 mmol, 74%). ^{1}H-NMR (C_6D_6): 7.96 (*s*, 1 arom. H); 7.92 (*s*, 1 arom. H); 7.65 (*s*, 2 arom. H); 7.61 (*s*, 2 arom. H); 1.88 (*s*, Me−C=N); 1.33 (*s*, Me−C=N); 0.98 (*s*, ^2J(Pt,H) = 80, PtMe). Anal. calc. for $C_{21}H_{27}ClN_2Pt$: C 33.46, H 2.01, N 3.72; found: C 33.15, H 1.75, N 3.44.

Data of (CyDAB^H)PtClMe (**2g**). Yellow solid. Yield 271 mg (0.58 mmol, 86%). ^{1}H-NMR (CD_2Cl_2): 8.89 (*s*, CH, ^3J(Pt,H) = 107); 8.45 (*s*, CH, ^3J(Pt,H) = 38); 4.34 (*m*, H−C=N); 4.21 (*m*, H−C=N); 2.21 (*m*, 4 H, CH$_2$); 1.87 (*m*, 4 H, CH$_2$); 1.75 (*m*, 2 H, CH$_2$); 1.45 (*m*, 6 H, CH$_2$); 1.21 (*m*, 4 H, CH$_2$); 1.34 (*s*, ^2J(Pt,H) = 79, PtMe). ^{13}C{^{1}H}-NMR (CD_2Cl_2): 161.6; 159.2; 67.1; 65.9; 35.0; 33.7; 26.2; 26.1; 26.1; 26.0; −13.4 (^1J(Pt,H) unresolved). ^{195}Pt{^{1}H}-NMR (CD_2Cl_2): −1111. Anal. calc. for $C_{15}H_{27}ClN_2Pt$: C 38.67, H 5.84, N 6.01; found: C 38.36, H 5.74, N 5.95.

Data of (CyDAB^{Me})PtClMe (**2h**). Yellow solid. Yield 294 mg (0.59 mmol, 88%). ^{1}H-NMR (CD_2Cl_2): 4.37 (*m*, H−C=N); 4.14 (*m*, H−C=N); 2.86 (*m*, CH$_2$); 2.03 (*m*, CH$_2$); 1.96 (*s*, Me−C=N); 1.84 (*s*, Me−C=N); 1.84 (*m*, CH$_2$); 1.67 (*m*, CH$_2$); 1.54 (*m*, 2 CH$_2$); 1.42–1.22 (*m*, 4 CH$_2$); 1.18 (*s*, ^2J(Pt,H) = 77, PtMe). ^{13}C{^{1}H}-NMR (CD_2Cl_2): 174.9; 171.5; 67.8; 66.1; 30.6; 30.2; 26.0; 25.8; 25.7; 25.3; 22.7; 18.8; −12.4 (^1J(Pt,C) = 717). ^{195}Pt{^{1}H}-NMR (CD_2Cl_2): −1225. Anal. calc. for $C_{17}H_{31}ClN_2Pt$: C 41.33, H 6.33, N 5.67; found: C 41.10, H 6.25, N 5.22.

Data of (CyDAB^H)PtI$_2$Me$_2$ (**4g**). Orange-yellow solid. Yield 62 mg (0.088 mmol, 80%). ^{1}H-NMR (CD_2Cl_2): 8.54 (*s*, ^3J(Pt,H) = 32, 2 CH); 4.13 (*m*, 2 H−C=N); 2.31 (*m*, 2 CH$_2$); 2.16 (*s*, ^2J(Pt,H) = 85, PtMe$_2$); 1.90 (*m*, 2 CH$_2$); 1.74 (*m*, CH$_2$); 1.45 (*m*, 4 CH$_2$); 1.22 (*m*, CH$_2$). ^{13}C{^{1}H}-NMR (CD_2Cl_2): 161.7; 66.6; 34.9; 26.1; 26.0; −13.9 (^1J(Pt,C) = 506). ^{195}Pt{^{1}H}-NMR (CD_2Cl_2): −1150. Anal. calc. for $C_{16}H_{30}I_2N_2Pt$: C 27.48, H 4.32, N 4.01; found: C 27.01, H 4.27, N 3.73.

Data of (CyDAB^H)PtICl(OMe)Me$_2$ (**7g**). Yellow solid. Yield 50 mg (0.10 mmol, 95%). ^{1}H-NMR (CD_2Cl_2): 8.61 (*s*, ^3J(Pt,H) = 26, 2 CH); 4.05 (*m*, 2 H−C=N); 2.76 (*m*, ^3J(Pt,H) = 61, MeO); 2.26 (*m*, CH$_2$); 2.10 (*m*, CH$_2$); 1.90 (*m*, 2 CH$_2$); 1.74 (*m*, CH$_2$); 1.61 (*s*, ^2J(Pt,H) = 72, PtMe$_2$); 1.45 (*m*, 3 CH$_2$); 1.33 (*m*, CH$_2$); 1.22 (*m*, CH$_2$). ^{13}C{^{1}H}-NMR (CD_2Cl_2): 160.8; 65.4; 33.8; 32.9; 26.0; 25.9; −0.98 (^1J(Pt,C) = 639). ^{195}Pt{^{1}H}-NMR (CD_2Cl_2): −1206. Anal. calc. for $C_{17}H_{33}I_2N_2OPt$: C 39.88, H 6.50, N 5.74; found: C 40.31, H 6.40, N 5.84.

Data of [(CyDAB^H)PtClMe$_2$MeCN)]$^+_2$[PtCl$_6$]$^{2-}$ (**9g**). Yellow solid. Yield 96 mg (0.066 mmol, 60%). ^{1}H-NMR (CD_2Cl_2): 9.55 (*s*, ^3J(Pt,H) = 29, CH); 3.90 (*m*, 2 H−C=N); 2.71 (*m*, MeCN); 2.17 (*m*, 2 CH$_2$); 1.93 (*m*, 3 CH$_2$); 1.76 (*s*, ^2J(Pt,H) obscured, PtMe$_2$); 1.74 (*m*, CH$_2$); 1.43 (*m*, 2 CH$_2$); 1.28 (*m*, 2 CH$_2$). ^{13}C{^{1}H}-NMR (CD_2Cl_2): 166.5; 66.9; 32.7; 32.7; 26.0; 25.9; 25.9; 25.8; 6.5; −0.32 (^1J(Pt,C) = 488). Anal. calc. for $C_{36}H_{70}Cl_8N_6Pt_3$: C 29.70, H 4.85, N 5.77; found: C 29.52, H 4.44, N 4.41.

Data of (TMEDA)PtI$_2$Me$_2$. Yellow solid. Yield (52 mg, 0.088 mmol, 80%). ^{1}H-NMR (CD_2Cl_2): 3.10 (*s*, ^3J(Pt,H) = 15, 12 H, NMe_2); 2.84 (*s*, ^3J(Pt,H) = 7.5, 2 NCH_2); 2.40 (*s*, ^2J(Pt,H) = 73, $PtMe_2$). ^{13}C{^{1}H}-NMR (CD_2Cl_2): 62.2; 54.0; −19.8 (^1J(Pt,C) = 493). ^{195}Pt{^{1}H}-NMR (CD_2Cl_2): −1559. Anal. calc. for $C_8H_{22}I_2N_2Pt$: C 16.14, H 3.73, N 4.71; found: C 16.20, H 3.82, N 4.67.

X-Ray Crystallographic Analysis. Data were collected on an *Enraf-Nonius CAD-4* diffractometer with the CAD-4 software package [47] and graphite monochromated MoKα radiation at 85 K. *Table 5* summarizes the crystallographic data[1]). The data processing, solution and refinement were done with SHELXS-93 [48] and SHELXL-97 [49] programs.

A suitable crystal of complex **9b** was grown from a sat. soln. of MeCN containing excess K_2PtCl_6. The cell constants were obtained by centering 25 reflections ($15.0^\circ < 2\theta < 24.6^\circ$). The *Laue* symmetry of 2/*m* was determined by merging symmetry-equivalent positions. The data were collected in the θ range of 1.3° to 25.0° ($-39 \le h \le 36, -11 \le k \le 11, -24 \le l \le 24$) in the ω scan mode. Three standard reflections were measured every 60 min and showed negligible decay of the crystal. No attempt was made to locate the H-atoms. For space group *C*2/*c*, there are 8 general positions, *i.e.*, 8 molecules in the unit cell. The unit-cell contains 4 molecules of $PtCl_6$, each sitting on a special position. Therefore, the list of atomic coordinates contains only one-half of a $PtCl_6$. The monocation lies on a general position; the dianion on a center of symmetry. For each cation, there is a disordered MeCN molecule. There are also 8 molecules of MeCN as a solvent of crystallization in the unit cell. This molecule of MeCN is disordered between two sites (51.4 : 48.6; constrained to a total population of 1) and forms a V pointing toward the cation and sharing a common Me group. The Me groups are not exactly at the same site, resulting in a fairly large displacement ellipsoid and shortened Me−C bond lengths. The six half-H-atoms were ignored; the Me C-atom was refined anisotropically and the other four partial solvent atoms were refined isotropically. Therefore, the list of atomic coordinates contains the positions of two MeCN moieties. During data collection, the crystal fell off. As a result, ψ-scans were not made and the crystal size was not measured. No absorption correction could be made due to lack of ψ-scan data. Consequently, the residual electron excursions are rather large (2.96 e$^-$Å^{-3} at 1.13 Å from Pt(1), 2.89 e$^-$Å^{-3} at 1.08 Å from Pt(1), 2.88 e$^-$Å^{-3} at 1.09 Å from Pt(2), −2.06 e$^-$Å^{-3} at 0.86 Å from Pt(1) as well as *ca.* 18 other peaks greater than 1 e$^-$Å^{-3} in magnitude).

A suitable crystal of complex **9g** was grown from a sat. soln. of MeCN/p.e. The cell constants were obtained by centering 25 reflections ($27.2^\circ < 2\theta < 28.0^\circ$). The *Laue* symmetry of $\bar{1}$ was determined by merging symmetry-equivalent positions. The data were collected in the θ range of 1.5° to 25.0° ($-11 \le h \le 11, -12 \le k \le 12, -16 \le l \le 15$) in the ω scan mode. Three standard reflections were measured every 75 min and showed no decay of the crystal. An empirical absorption correction was applied to the data based on the ψ scans data (8.343 mm^{-1}) with CRYM[50]. H-Atoms were refined anisotropically and all H-atoms placed at calculated positions with U_{iso} at 120% of the U_{eq} of the attached atom. During least-squares refinement, the H-atoms on the MeCN of solvation were restrained to geometric positions with the C−H distances free to refine as a unit and with the torsion angle free to optimize the fit to electron density. The asymmetric unit contains the principal compound ($C_{18}H_{33}ClN_3Pt$) solvated by one molecule of MeCN and half a molecule of $PtCl_6$ (which sits on a center of symmetry). Therefore, the unit-cell contents appear to be A_2B with two MeCN solvates of crystallization. In the final difference *Fourier* synthesis, the electron density fluctuates in the range of +1.26 to −0.90 e$^-$Å^{-3}.

This work was supported by the *Department of Energy*, *Office of Industrial Technology*, *Akzo-Nobel Petrochemicals*, and *BP*.

---

[1]) Crystallographic data (excluding structure factors) for the structure(s) reported in this paper have been deposited with the *Cambridge Crystallographic Data Centre* as deposition No. CCDC-111741 for **9b** and No. CCDC-102762 for **9g**. Copies of the data can be obtained, free of charge, on application to the CCDC, 12 Union Road, Cambridge CB2 1EZ, UK (fax: +44(1223)336033; e-mail: deposit@ccdc.cam.ac.uk). Structure factors are available from the authors *via* e-mail: xray@caltech.edu.

REFERENCES

[1] N. F. Gol'dshleger, V. V. Es'kova, A. E. Shilov, A. A. Shteinman, *Zh. Fiz. Khim*. **1972**, *46*, 1353.
[2] B. A. Arndtsen, R. G. Bergman, T. A. Mobley, T. H. Peterson, *Acc. Chem. Res.* **1995**, *28*, 154.
[3] 'Selective Hydrocarbon Activation', Eds. J. A. Davies, P. L. Watson, J. F. Liebman, and A. Greenberg, VCH, New York, 1990.
[4] 'Activation and Functionalization of Alkanes', Ed. C. L. Hill, John Wiley & Sons, New York, 1989.
[5] R. A. Periana, D. J. Taube, E. R. Evitt, D. G. Loffler, P. R. Wentrcek, G. Voss, T. Masuda, *Science* **1993**, *259*, 340.
[6] L. C. Kao, A. C. Hutson, A. Sen, *J. Am. Chem. Soc*. **1991**, *113*, 700.
[7] J. A. Labinger, A. M. Herring, J. E. Bercaw, *J. Am. Chem. Soc*. **1990**, *112*, 5628.
[8] A. Sen, E. Gretz, T. F. Oliver, Z. Jiang, *New J. Chem*. **1989**, *13*, 755.
[9] E. Gretz, T. F. Oliver, A. Sen, *J. Am. Chem. Soc*. **1987**, *109*, 8109.
[10] S. A. Svejda, L. K. Johnson, M. Brookhart, *J. Am. Chem. Soc.* **1999**, *121*, 10634.
[11] S. A. Svejda, M. Brookhart, *Organometallics* **1999**, *18*, 65.
[12] S. Y. Desjardins, A. A. Way, M. C. Murray, D. Adirim, M. C. Baird, *Organometallics* **1998**, *17*, 2382.
[13] C. M. Killian, L. K. Johnson, M. Brookhart, *Organometallics* **1997**, *16*, 2005.
[14] C. M. Killian, D. J. Tempel, L. K. Johnson, M. Brookhart, *J. Am. Chem. Soc*. **1996**, *118*, 11664.
[15] L. K. Johnson, S. Mecking, M. Brookhart, *J. Am. Chem. Soc*. **1996**, *118*, 267.
[16] L. K. Johnson, C. M. Killian, M. Brookhart, *J. Am. Chem. Soc*. **1995**, *117*, 6414.
[17] F. C. Rix, M. Brookhart, *J. Am. Chem. Soc*. **1995**, *117*, 1137.
[18] M. Brookhart, F. C. Rix, J. M. Desimone, J. C. Barborak, *J. Am. Chem. Soc*. **1992**, *114*, 5894.
[19] S. S. Stahl, J. A. Labinger, J. E. Bercaw, *J. Am. Chem. Soc*. **1996**, *118*, 5961.
[20] M. W. Holtcamp, J. A. Labinger, J. E. Bercaw, *J. Am. Chem. Soc*. **1997**, *119*, 848.
[21] M. W. Holtcamp, L. M. Henling, M. W. Day, J. A. Labinger, J. E. Bercaw, *Inorg. Chim. Acta* **1998**, *270*, 467.
[22] L. Johansson, O. B. Ryan, C. Romming, M. Tilset, *Organometallics* **1998**, *17*, 3957.
[23] L. Johansson, O. B. Ryan, M. Tilset, *J. Am. Chem. Soc*. **1999**, *121*, 1974.
[24] L. Johansson, M. Tilset, J. A. Labinger, J. E. Bercaw, *J. Am. Chem. Soc*. **2000**, *122*, 10846.
[25] L. A. Kushch, V. V. Lavrushko, Y. S. Misharin, A. P. Moravsky, A. E. Shilov, *Nouv. J. Chim*. **1983**, *7*, 729.
[26] G. A. Luinstra, L. Wang, S. S. Stahl, J. A. Labinger, J. E. Bercaw, *Organometallics* **1994**, *13*, 755.
[27] G. A. Luinstra, L. Wang, S. S. Stahl, J. A. Labinger, J. E. Bercaw, *J. Organomet. Chem.* **1995**, *504*, 75.
[28] L. Wang, S. S. Stahl, J. Labinger, J. E. Bercaw, *J. Mol. Cat., A: Chem*. **1997**, *116*, 269.
[29] P. M. Gidney, R. D. Gillard, B. T. Heaton, *J. Chem. Soc., Dalton Trans.* **1973**, 132.
[30] W. B. Connick, V. M. Miskowski, V. H. Houlding, H. B. Gray, *Inorg. Chem*. **2000**, *39*, 2585.
[31] V. M. Miskowski, V. H. Houlding, *Inorg. Chem*. **1989**, *28*, 1529.
[32] V. M. Miskowski, V. H. Houlding, C.-M. Che, *Inorg. Chem*. **1993**, *31*, 2518.
[33] D. Manuta, A. Lees, *Inorg. Chem*. **1983**, *22*, 3825.
[34] W. de Graaf, J. Boersma, W. J. J. Smeets, A. L. Spek, G. van Koten, *Organometallics* **1989**, *8*, 2907.
[35] H. Taube, *Advan. Inorg. Chem. Radiochem.* **1959**, *1*, 1.
[36] W. R. Mason, *Coord. Chem. Rev*. **1972**, *7*, 241.
[37] S. Hasenzhal, H.-D. Hausen, W. Kaim, *Chem.–Eur. J.* **1995**, *1*, 95.
[38] A. Klein, W. Kaim, F. M. Hornug, J. Fielder, S. Zalis, *Inorg. Chem. Acta* **1997**, *264*, 269.
[39] R. J. Klingler, J. C. Huffman, J. K. Kochi, *J. Organomet. Chem*. **1981**, *206*, C7.
[40] M. Fusto, F. Giordano, I. Orabona, F. Ruffo, *Organometallics* **1997**, *16*, 5981.
[41] P. Ganis, I. Orabona, F. Ruffo, A. Vitagliano, *Organometallics* **1998**, *17*, 2646.
[42] R. van Asselt, C. J. Elsevier, W. J. J. Smeets, A. L. Spek, *Inorg. Chem*. **1994**, *33*, 1521.
[43] R. van Asselt, C. J. Elsevier, W. J. J. Smeets, A. L. Spek, R. Benedix, *Recl. Trav. Chim. Pay. B* **1994**, *113*, 88.
[44] J. M. Kliegman, R. K. Barnes, *J. Org. Chem*. **1970**, *35*, 3140.
[45] H. tom Dieck, M. Svoboda, T. Grieser, *Z. Naturforsch*. **1981**, *36b*, 823.
[46] G. S. Hill, M. J. Irwin, C. J. Levy, L. M. Rendina, R. J. Puddephatt, in 'Inorganic Synthesis', Ed. M. Y. Darensbourg, John Wiley & Sons, Inc., New York, 1998; Vol. 32; p. 149.
[47] CAD-4 Software, Version 5, Enraf-Nonius, Delft, The Netherlands. 1989.

[48] G. M. Sheldrick, 'SHELXS-97, Program for the Solution of Crystal Structures', University of Göttingen, 1997.
[49] G. M. Sheldrick, 'SHELXL-97, Program for the Solution of Crystal Structures', University of Göttingen, 1997.
[50] D. J. Duchamp, Proceedings of the American Crystallography Association Meeting, Bozeman, MT, 1964; p. 29.
[51] L. J. Farrugia, *J. Appl. Crys.* **1997**, *30*, 565.

Received July 10, 2001